Chapter 3

Structural, mechanical and gas barrier properties of poly(ethylene terephthalate) nanohybrid using nanotalc

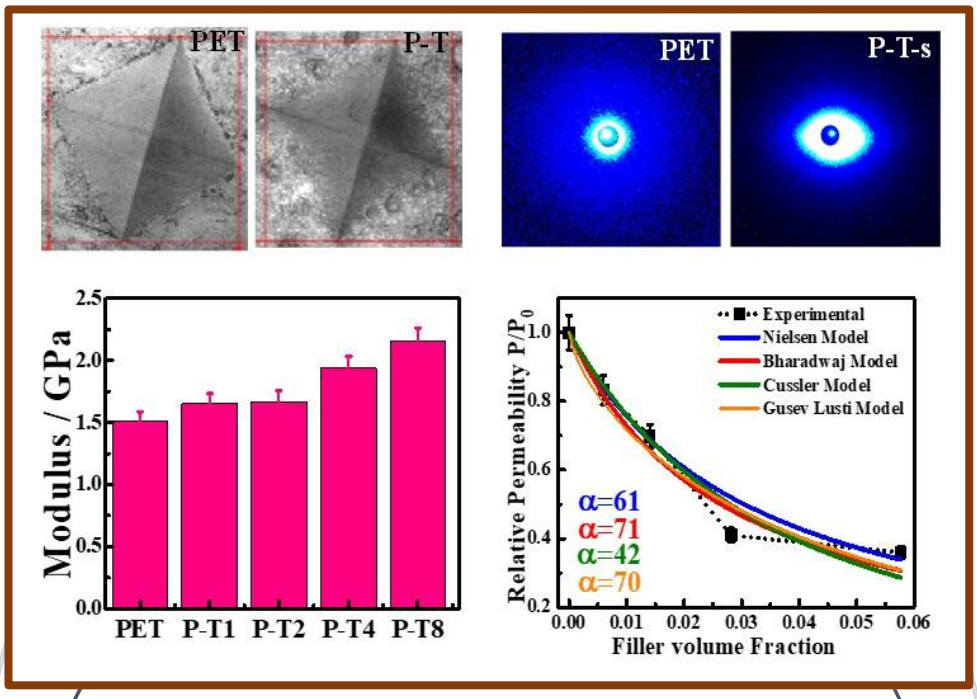

3.1. Introduction

The example of fillers which have been used in the past to enhance the various properties of polymers (such as mechanical, thermal and permeability properties) of the PET are Cloisite 15A, Nanolin DK2 [109], Cloisite 30B [94], Fluoromica [101], phosphate glass [164], silica [106], alumina [165], and so forth. Talc is a layered silicate which is used as filler for composite materials for reduction of production costs and for improving their chemical and physical properties such as mechanical, gas barrier, lubricating properties, and so forth. It is used in various industrial applications [166]. Nanotalc is a layered phyllosilicate having 2:1 layered structure composed of one octahedral magnesium ($Mg_{12}O_{12}H_4$) brucite sheet sandwiched between two tetrahedral silica sheets. It has a molecular formula of $Mg_3Si_4O_{10}(OH)_2$. The layers of nanotalc are electrically neutral and are connected together by weak Van der Waals forces. Because of these weak adhesion, the silica and brucite sheets slide over each other [167-169].

Various polymer clay hybrids have been studied widely [16, 170-174] as the filler needed is much less in quantity to improve the properties to a great extent and the preparation techniques are comparatively easier and less energy consuming process. In previously reported studies, talc is used with PET but mostly in microform or macroform [175-178]. Yamada et al. [175] used microtalc to improve the thermal resistance of recycled PET blend. The samples were prepared through melt blending technique. The modulus increased by 25% using 20 wt% of microtalc. Haubruge et al. [176] used macrotalc for the epitaxial nucleation of PET. The structure at the lattice and lamellar scales was studied. Sekelik et al. [177] reported macrotalc for reduction of barrier property of PET and its copolymer using the

microlayering technique to prepare the film and 32 wt% of talc was used to improve the barrier property. Other reports have been published to improve the mechanical and other properties of polypropylene [178, 179], polyamides [179, 180], polyurethane [181], and so forth.

Here, in this work, nanotalc has been used to study the effect on thermal stability, microhardness, improving the mechanical property, gas barrier property using a meager amount of nanotalc as compared to the previously reported studies. Further, the structural development especially under uniaxial elongation has been studied through small-angle X-ray scattering (SAXS) which shed light on the properties of the nanohybrid under deformation.

3.2 Experimental

3.2.1 Materials: PET, nanotalc clay, DCM as solvent.

Nanotalc was supplied by Soap Stone Pvt. Ltd., India.

PET nanohybrids have been prepared via solvent casting route as explained in ***Chapter 2*** and abbreviated as P-T1, P-T2, P-T4, P-T8 for 1, 2, 4 and 8 weight percentage of nanoclay concentrations. Abbreviation P-T have been used for the 4% of clay concentration.

3.3 Results and discussion

3.3.1 Dispersion and interactions

The nanoclay platelets get dispersed in the polymer matrix and their homogeneous dispersion as well as intercalation is desirable for nanohybrid structure formation for various properties

enhancements. Level of dispersion of nanotalc in polymer matrix has been examined through bright field TEM images as shown in ***Figure 3.1a***. The dispersion of nanotalc in the polymer matrix has been found to be homogenous, although there are some agglomerations [182]. Agglomerations cause improvement in rigidity but they also cause decrement in other mechanical properties such as mechanical strength and elongation at break [2]. The dispersion of nanotalc in the PET matrix is similar to the other reports [94, 98]. The evaluation of average geometric dimensions has been measured from the TEM image. The average aspect ratio (ratio of length to width) has been estimated to be 12 whereas average correlation length (distance between two nanoparticles) has been measured to be 480 nm [171, 172].

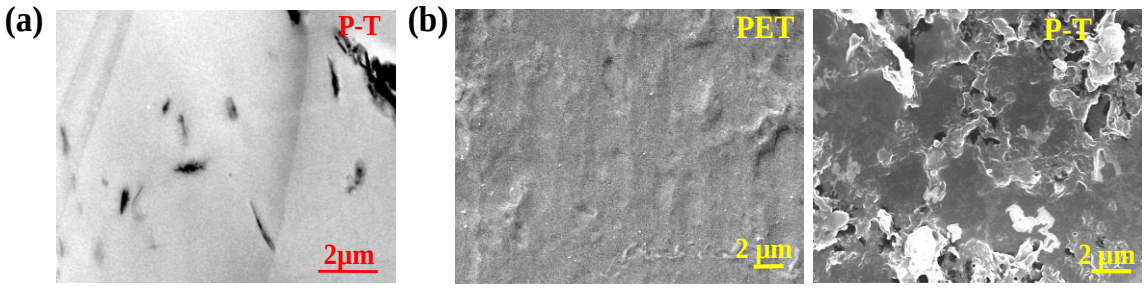

Figure 3.1: (a) *Dispersion of nanotalc in PET matrix using bright field TEM image;* ***(b)*** *SEM images showing surface morphology of PET and P–T nanohybrid containing 4 wt % of filler*

SEM images have been taken to understand the surface morphology of pure PET and P–T nanohybrids which are shown in ***Figure 3.1b***. The nanohybrids have roughened morphology in comparison to pristine PET because of the presence of nanotalc clay. The interplanar distanced of talc platelets have been observed through XRD patterns shown in ***Figure 3.2a***. The nanotalc clay shows a peak $2\theta = 9.42°$ which corresponds to an interplanar distance of

0.9 nm (d_{001}), which is the characteristic peak of nanotalc (***Figure 3.2b***). There is no change of peak position in nanohybrid, as compared to nanotalc, implying no intercalation of polymer inside the nanotalc layers. The reason lies in the much larger radius of gyration of PET molecules (3 nm) in comparison to interplanar distance of talc (0.9 nm) and comparatively less expanding behavior of nanotalc platelets [183]. Thus, the polymer chains are unable to enter into the galleries of nanotalc but the intensity of the said peak enhances with nanotalc content in the hybrid presumably due to greater coherency. However, the good dispersion of filler should lie on the interaction between talc and PET chains. The strong interaction of nanotalc with PET matrix can be observed through ultraviolet–visible (UV–vis) spectroscopy ***Figure 3.2c***. The pure PET has an absorption peak at 300 nm whereas the P–T nanohybrids show the peak at 293 nm. This blue shifting at lower wavelength is due to $n \rightarrow \pi^*$ transition where a nonbonded electron of oxygen atom is excited to π^* orbital because of the strong interactions of nanotalc with polymer matrix [184]. Further, to perceive the nature of the interaction, FTIR has been shown in ***Figure 3.2d***. The strong peak at 1707 cm^{-1} in PET has been attributed to symmetric stretching of ester bond (−C=O). This peak is slightly shifted to 1708 cm^{-1} in P–T nanohybrids because of the interaction of PET and nanotalc platelets. The band at 1022 cm^{-1} is assigned to aromatic ring C−H plane bending. This peak shifts to 1017 cm^{-1} in the presence of nanotalc. The band at 867 cm^{-1} is associated with parasubstituted benzene ring, C−H out of plane vibration. This peak is shifted to 862 cm^{-1} in the presence of nanotalc due to interaction of PET and nanotalc. The absorption band at 1244 cm^{-1} is attributed to (C=O)−C stretching of ester, ring ester in plane mode which is shifted to 1239 cm^{-1} in P–T nanohybrids. The absorption band at 1528 cm^{-1} is associated with the parasubstituted benzene ring, C−C stretching, C−H in plane vibrations.

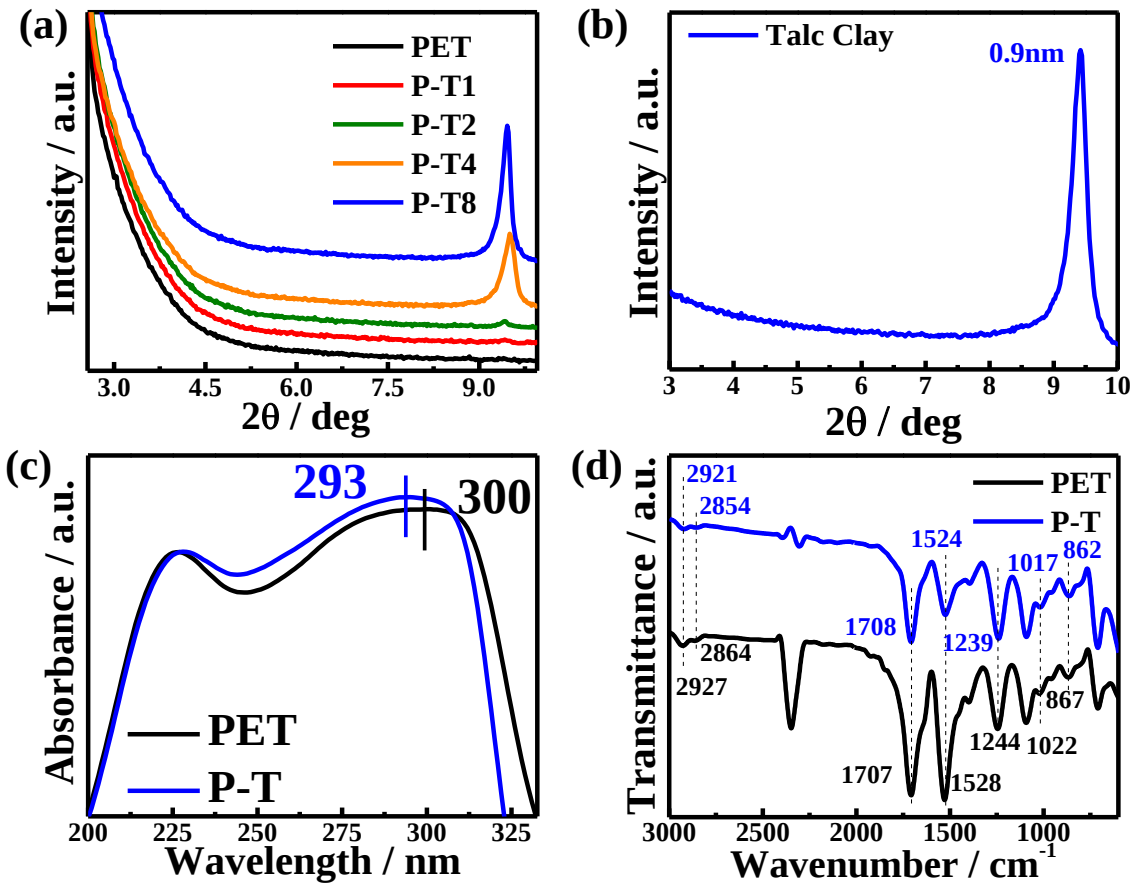

Figure 3.2: ***(a)*** *XRD patterns of PET and its nanohybrids with different weight concentrations of filler. The numbers after P–T indicate the nanotalc content (wt %) in the hybrid;* ***(b)*** *XRD pattern of pure nanotalc clay;* ***(c)*** *UV–vis absorption spectra of PET and its nanohybrid for 4 wt % filler; and* ***(d)*** *FTIR spectra of pristine PET and nanohybrid containing 4 wt % filler.*

This band is shifted to 1524 cm^{-1} in the presence of nanotalc. The band at 2864 and 2927 cm^{-1} are attributed to aromatic and aliphatic C−H bond stretching which shift to 2854 and 2921 cm^{-1}, respectively, in P–T nanohybrids [185, 186]. From the shifting of FTIR peaks, it appears that dipolar interaction predominantly occurs between talc dipole (metal-oxygen link) and π-electron cloud of benzene ring in PET chains.

3.3.2 Thermal properties and stability

Figure 3.3a shows the TGA curve of pure PET and P-NK nanohybrid. The curve was plotted between weight loss measurement as a function of temperature.

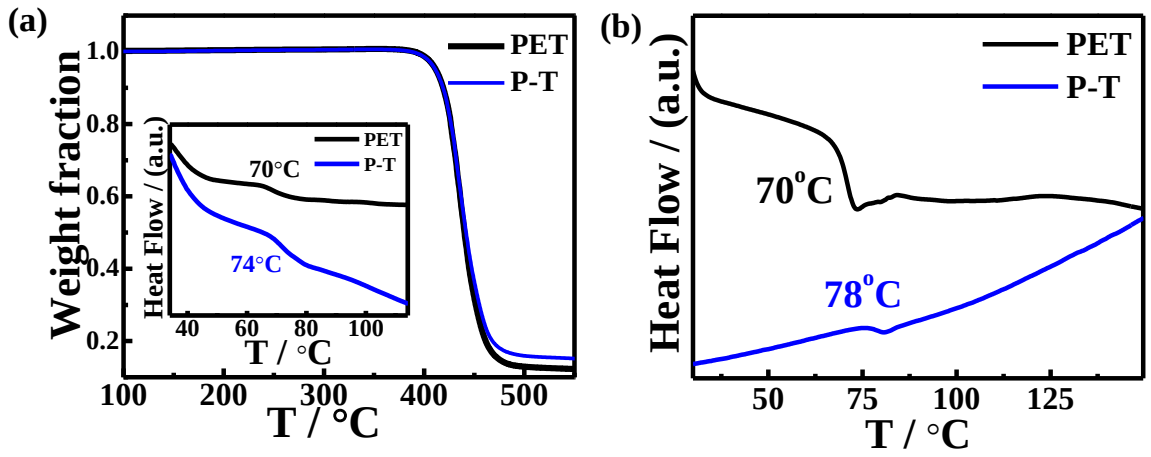

Figure 3.3: (a) *TGA thermograms of PET and its nanohybrids showing thermal stability of nanohybrid of 4 wt % filler concentration, inset image shows the glass-transition temperatures of pure PET and its nanohybrid using DTA thermogram; and* ***(b)*** *DSC thermograms of pristine PET and its nanohybrid of 4 wt % filler concentration.*

The degradation temperature (T_d) was taken as the temperature which was associated to 5% of weight loss. T_d of PET and P–T nanohybrid is found to be 410 °C indicating no loss of degradation temperature in the presence of nanotalc which has advantage over other organically modified nanoclay as organic part degrade at lower temperature as reported in previous study [91]. The glass-transition temperature (T_g) has been observed through DTA thermograms (inset image of ***Figure 3.3a***) where P–T nanohybrid has a higher glass-transition temperature of 74 °C against 70 °C for pure PET. The increment in glass transition temperature in nanohybrids has also been confirmed from the DSC thermograms in ***Figure 3.3b*** where nanohybrid exhibits glass-transition temperature of 78 °C vis-à-vis 70 °C of pure

PET. The glass-transition temperature shows the increment in the movement of the polymer segment and nanotalc imparts stiffness by creating hindrance in the movement of polymer chains arising from the good interaction as discussed above.

3.3.3 Mechanical responses

The nanohybrids have been tested for their mechanical strength in wide range of filler concentration. ***Figure 3.4a*** shows the stress–strain curves of PET and its representative nanohybrid. The Young's modulus of nanohybrids is determined from the linear region of the stress–strain curve. The Young's modulus has been found to be increasing with the increasing concentration of nanotalc (***Figure 3.4b***). The Young's modulus has been increased by 43% for 8 wt % of filler concentration as compared to pure PET. The modulus increment is considerably higher than previously reported values [94, 175]. The increment in the Young's modulus is due to the reinforcing effect of nanotalc along with the formation of a superstructure resulted after achieving a percolation threshold [91]. The restriction in the movement comes into effect as the concentration of nanotalc increased. Specifically, the mechanical properties of nanohybrids (such as stiffness, strength, toughness, and elongation at break) depend on the dispersion, interfacial strength, affinity of components, spatial organization as well as specific surface area, aspect ratio, organization, and nanofiller content [1]. As the deformation proceeds, the agglomerates trap and disturb the elementary paths of the polymer chains. This results in the enhanced particle-chain entanglement network [101, 187]. Here, good particle–polymer interaction is taken place as the imperative condition for this effect.

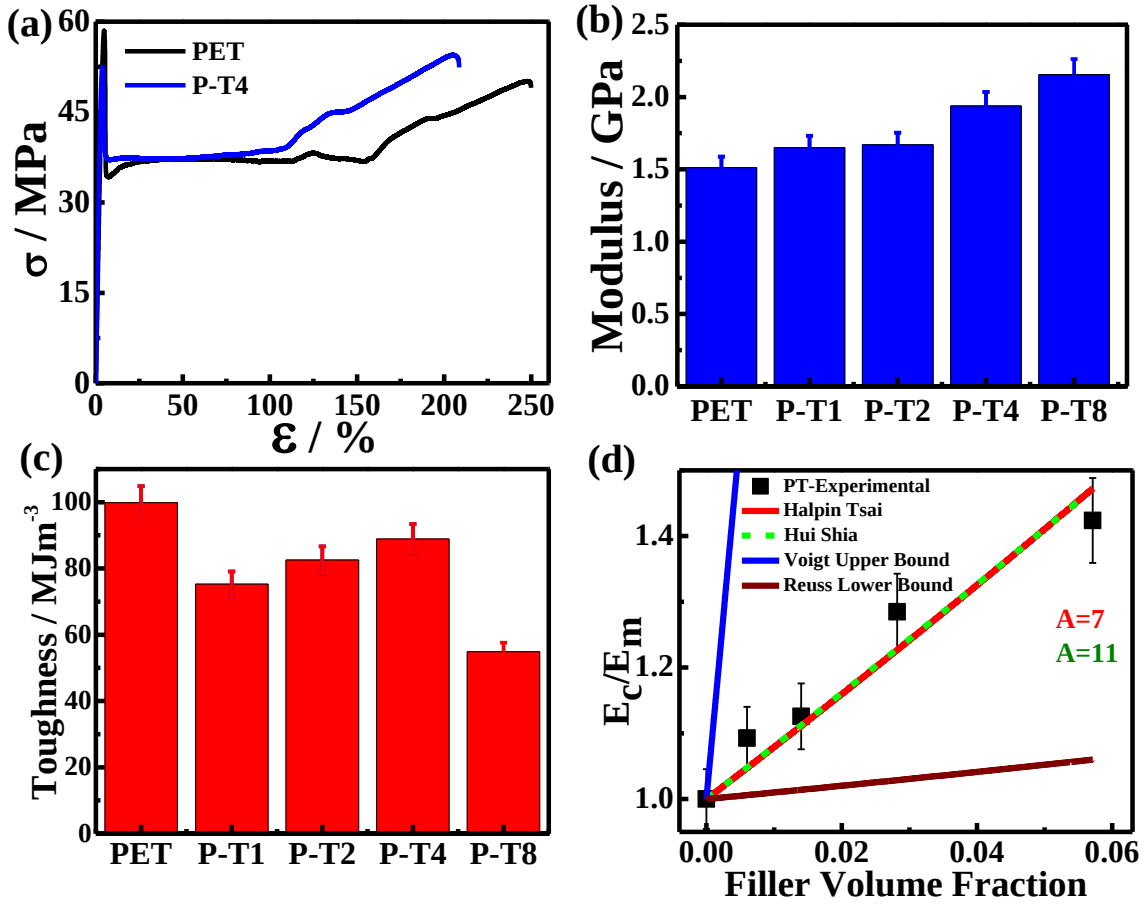

Figure 3.4: ***(a)*** *Stress–strain curves of PET and its nanohybrid containing 4 wt % of filler concentration;* ***(b)*** *Improvement in modulus values in P–T nanohybrids for different amount of filler loading comparing pure PET. The number after P–T indicates the nanotalc content (wt %) in the hybrid;* ***(c)*** *variation in toughness values as a function of filler concentrations; and* ***(d)*** *predictions of modulus values using different micromechanical models as indicated.*

Moreover, the polymer nanohybrids have the clusters and large tactoids present in the system which can act as the crack propagation center and, hence, can be the reason behind premature breaking of the nanohybrid samples [91]. The modulus increases with increased nanotalc incorporation while the elongation at break reduces slightly as expected because of the increased mechanical rigidity. However, the toughness, as measured from the area under

stress–strain curve, exhibits certain reduction having optimum value for 4 wt % nanotalc containing hybrid (***Figure 3.4c***). The nanohybrid having 4% talc has shown 28% of modulus increment and only 11% reduction in toughness as compared to pure PET while most of the composites using commercial clay exhibited drastic reduction in toughness, as the elongation at break reduced significantly up to 90% as reported in previous studies [94, 96, 98]. Hence, the nanohybrid prepared have found to have increased modulus while retaining toughness for practical usages such as sports, packaging, and so forth.

3.3.4 Modulus prediction by micro mechanical models:

Halpin Tsai and Hui Shia models have been used for the modulus prediction studies as shown in ***Fig. 3.4d***. Halpin Tsai model is widely used for the fiber reinforced composites for prediction of tensile modulus as a function of filler volume fraction and aspect ratio [188, 189].

This takes into account the effect of unidirectional as well as random fiber orientation with variation of aspect ratio. These models take average particle size into account because of the variation of the size dispersion in the polymer matrix. This model is widely used for a different variety of fillers geometry that includes fiber-like or flake-like as well as disk-like platelets. The Halpin Tsai model is given as [188]:

$$\frac{E_c}{E_m} = \frac{1+\zeta\eta\varphi_f}{1-\eta\varphi_f} \tag{3.1}$$

$$\eta = \frac{\frac{E_f}{E_m}-1}{\frac{E_f}{E_m}+\zeta} \tag{3.2}$$

Where, E_c, E_m, E_f are elastic modulus of composite material, polymer matrix, and filler respectively. ζ =2A=2(ℓ/t) for disk like platelets, ℓ being the length and t is thickness of clay particle. Hence, ζ is a shape parameter which depends on loading direction, filler geometry and aspect ratio. The filler volume fraction is calculated by the equation below.

$$\phi_f = \frac{W_f}{W_f + (1 - W_f)\frac{\rho_f}{\rho_m}} \tag{3.3}$$

where, ϕ_f and W_f are the volume fraction and weight fraction of the nanoclay, respectively. ρ_f and ρ_m are the densities of the filler and the matrix, respectively. The variation of nanoclay weight fraction is taken from 1 to 8%. Hui-Shia model is a prediction of elastic modulus for unidirectionally oriented fiber in a two phase composite which is reinforced with fiber-like or flake like inclusions. The perfect interfacial bonding between polymer matrix and filler is taken as an assumption in this model [189, 190].

$$\frac{E_c}{E_m} = \frac{1}{1 - \frac{\phi}{4}\left[\frac{1}{\xi} + \frac{3}{\xi + \Lambda}\right]} \tag{3.4}$$

where,

$$\xi = \phi + \frac{E_m}{E_f - E_m} + 3\left(1 - \phi_f\right)\left[\frac{(1-g)\alpha^2 - \frac{g}{2}}{\alpha^2 - 1}\right]$$

$$g = \frac{\pi}{2}\,\alpha$$

$$\Lambda = \left(1 - \phi_f\right)\left[\frac{3(\alpha^2 + 0.25)g - 2\alpha^2}{\alpha^2 - 1}\right]$$

Where, α is inverse aspect ratio. For the disc like platelets α = 1/A = (d / ℓ). The range of values taken for α is less than 0.1. Voigt upper bound and Reuss lower bound models give

the range of maximum and minimum fitting values for the elastic modulus of the nanohybrid. When ζ reaches to infinity, Halpin Tsai model reaches to a maximum value called upper bound. Here, aligned fibers and the matrix are assumed to have same uniform strain in the fiber direction. The effective modulus is given by Voigt as [191]:

$$E_c = \phi E_f + (1-\phi) E_m \tag{3.5}$$

when, ζ is taken as 0, the Halpin Tsai equation reaches to a minimum value under equal stress called isostress approach given as Reuss inverse rule of mixture [189]:

$$\frac{1}{E_c} = \frac{\phi_f}{E_f} + \frac{(1-\phi_f)}{E_m} \tag{3.6}$$

The experimental values have been fitted with Halpin-Tsai and Hui-Shia models (***Figure 3.4d***). A good correlation between experimentally obtained values and theoretical models are obtained. It is observed that the increasing aspect ratio of the inorganic talc fraction results in the significant enhancement of the nanohybrid modulus values. The values obtained by Halpin-Tsai model shows satisfying agreement with the experimental values. The best fit for increasing modulus with increment of filler incorporation into the polymer matrix is obtained with the value of aspect ratio as 7. However, the average aspect ratio calculated from the TEM images is ~12 (results from the tactoid formations). The experimental values being slightly less than the predicted values could be because the nanotalc platelets are not fully exfoliated. The elastic modulus of nanotalc taken as filler modulus is the value for one layer of the nanotalc which decreases with the formation of tactoids. Moreover, the experimental values also depend upon the loading direction relative to the orientation of the filler particles, filler geometry, and aspect ratio. Hui-Shia model also fits well for an aspect ratio of 11. The

deviation in fitting values could be because at higher percentage of talc loading, the number of talc particles also increase which results in decrement of the aspect ratio of the nanotalc. This happens presumably due to the tactoid formation because of increased number of platelets. Hui-Shia model considers the perfect interfacial bonding between the filler and the matrix and takes the unidirectional fiber orientation whereas in these nanohybrids, the nanotalc particles are dispersed in a random fashion. On the other hand, Halpin-Tsai model does not consider the interfacial interaction and, hence, we get the different values of aspect ratios for the fitting curves of both the models. When the material is stretched, the stacking structure of the talc nanoparticles could have been distorted. This stretched distorted structure would result in the elongated talc nanoparticles having higher aspect ratio with same number of layers per stack. Nonetheless, there is no fixed value of aspect ratio for which the model fits perfectly. The reason for this deviation is the ideal assumptions taken such as identical filler geometry, perfect interfacial interaction with no interfacial slip, matrix cracking, matrix-filler debonding, and so forth. The maximum and minimum values of elastic modulus have been fitted using eqs. (6) and (7). The elastic modulus value of nanohybrid always lies between these curves. Moreover, the Halpin Tsai and Hui Shia models are best suited for the system as both the models predict values very closely at aspect ratio values of 7 and 11, respectively.

3.3.5 Microhardness of the nanohybrids

The nanohybrids have the talc platelets which are present in the form of tactoids. For obtaining the reliable hardness values, the imprint for each load should be larger than the dimension of talc tactoids present in the nanohybrid [192, 193]. The talc has the dimension

range of 100–500 nm. The impressions of diamond indenter on the PET and P–T nanohybrid are shown in ***Figure 3.5a***. The impressions of nanohybrids are comparatively darker than pristine PET because of the presence of nanotalc. The average diameter of the impression is used to calculate the Vicker hardness value. Microhardness values obtained for the samples are shown in ***Table 3.1*** as a function of filler concentration. The hardness of the nanohybrids increases in a linear fashion with increasing the amount of filler incorporation. The hardness increases up to 2.8% for 8 wt % of nanotalc. The microhardness of the nanohybrid is related closely with the macro mechanical characteristics of the nanohybrids. The hardness value is linearly dependent on the elastic modulus of the material. The reason behind this enhancement of hardness is comparatively higher hardness of talc than of pure PET as well as the good dispersion of nanotalc in the polymer matrix. The increment in hardness of the nanohybrid depends on the strong bonding of the filler particles and polymer matrix so that better stress transfer occurs under loading. Moreover, the talc particles can form a network structure which causes the enhanced stiffness in the nanohybrid resulting increased hardness values of the nanohybrid [194].

Table 3.1: *Vicker hardness values for PET and P-T nanohybrids*

Sample	Vicker Hardness
PET	11.58
P-T1	11.75
P-T2	11.78
P-T4	11.78
P-T8	11.89

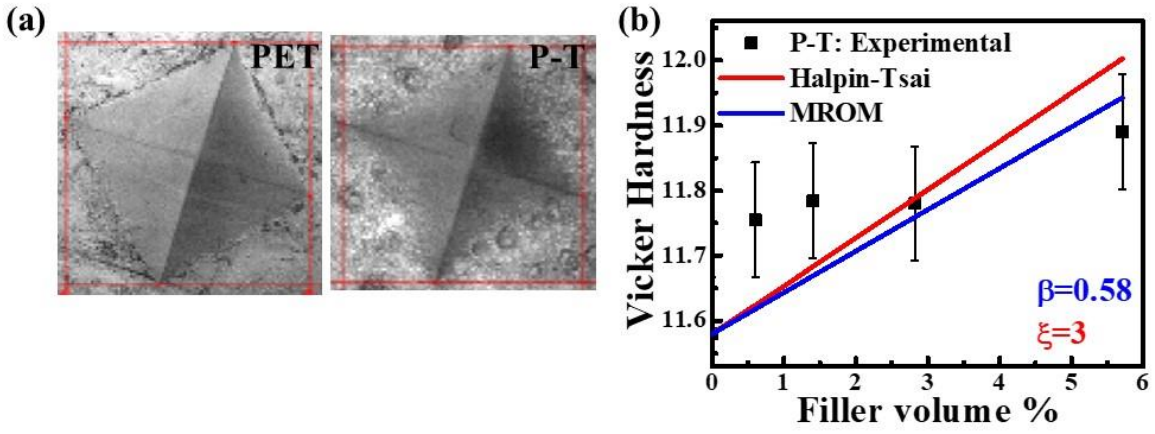

Figure 3.5: (a) *impressions of indenter created through Vicker hardness test of pure PET and its nanohybrid containing 4 wt % of filler concentration; and* ***(b)*** *fitting of hardness values using different micromechanical models as indicated.*

3.3.6 Theoretical modeling of hardness

The experimental curve has been fitted with theoretical models predicted by the modified rule of mixtures (MROM) given as [193, 195].

$$H_c = \beta H_f \phi_f + H_m \phi_m \tag{3.7}$$

Where, H_c, H_f and H_m are the hardness values for nanohybrid, filler and matrix, respectively. β depends upon the aspect ratio and filler particle reinforcements in the polymer matrix. It is taken as strengthening efficiency factor. ϕ_f and ϕ_m are taken as the volume fraction of clay particles since the properties of the nanohybrid depends on the volume occupied by the reinforcing filler [195]. For prediction of the mechanical properties of the hybrids containing different shapes and types of filler materials, modified Halpin Tsai equation [195] has been used. This equation has been applied to predict the microhardness values of the nanohybrids.

For randomly oriented nanoplatelets, the microhardness value can be predicted by the eqn. below

$$H_c = H_m \left[\frac{1+\xi\eta\phi_f}{1-\eta\phi_f}\right] \tag{3.8}$$

where, $\eta = [(H_f/H_m-1)/(H_f/H_m+\xi)]$, H_c, H_m, H_f are the hardness values for the nanohybrid, polymer matrix and the filler particles, respectively, and ϕ_f is the volume fraction of the filler element which is obtained by using equation (4). ξ is an adjustable parameter which depends upon the particles geometry, dimensions and loading direction relative to the filler particle orientation. For the upper bound, ξ is taken as infinite and for the lower bound, $\xi = 0$. However, ξ is an adjustable curve fitting parameter. It can be seen from ***Figure 3.5b*** that Halpin Tsai model fits at $\xi = 3$, whereas MROM model fits well with the experimental values at $\beta = 0.58$. The models fit well at an input hardness value of filler taken as 20 VHN. It has been observed in previous reports that lower the difference in the values of matrix and filler hardness, higher will be the values of fitting parameters [195]. Hence, the curve fits at comparatively higher values of fitting parameters. The MROM model shows good agreement with the experimental data. On the other hand, Halpin Tsai equation slightly over predicts the hardness. This difference in the theoretical and experimental values is due to the lower difference in hardness values of the nanotalc and polymer matrix in the presence of defects, voids, agglomeration of talc particles as well as the variation in the geometrical dimensions of the talc particles.

3.3.7 Temperature dependent viscoelastic properties

The Mechanical properties under dynamic condition as measured through DMA provide storage modulus (*E'*), loss modulus (*E''*) and loss tangent (tanδ) as a function of temperature (***Figure 3.6a, b and c***). The storage modulus is indicative of the elastic modulus whereas the loss modulus illustrates the energy lost. The damping factor tanδ is calculated through the ratio of loss modulus to the storage modulus.

The PET has mainly two relaxations namely α and β along with a rubbery plateau followed by flowing (melting) region. The β relaxation is associated with the glassy region where macromolecules are present in a frozen state and their segmental motions are restricted [196]. This relaxation is found at low temperatures (around -70°C) and has not been discussed here in this work. The α relaxation is found at high temperatures and corresponds to the glass transition temperature (T_g).

The storage modulus of PET and PET nanohybrids have been shown in ***Figure 3.6a***. At room temperature, the *E'* values of P-T4 and P-T8 were 45% and 50% higher respectively as compared to pristine PET. As the temperature increases, the storage modulus of PET starts decreasing at around 72°C and the decrement is quite steep which indicates the homogeneous structure of pure PET. The PET nanohybrids show higher *E'* values than the pure PET at lower temperatures because of the high stiffness of nanohybrids due to the presence of nanoclay of higher modulus. This have also been supported by the higher tensile modulus results of nanohybrids at room temperature as elaborated in 'mechanical responses' section.

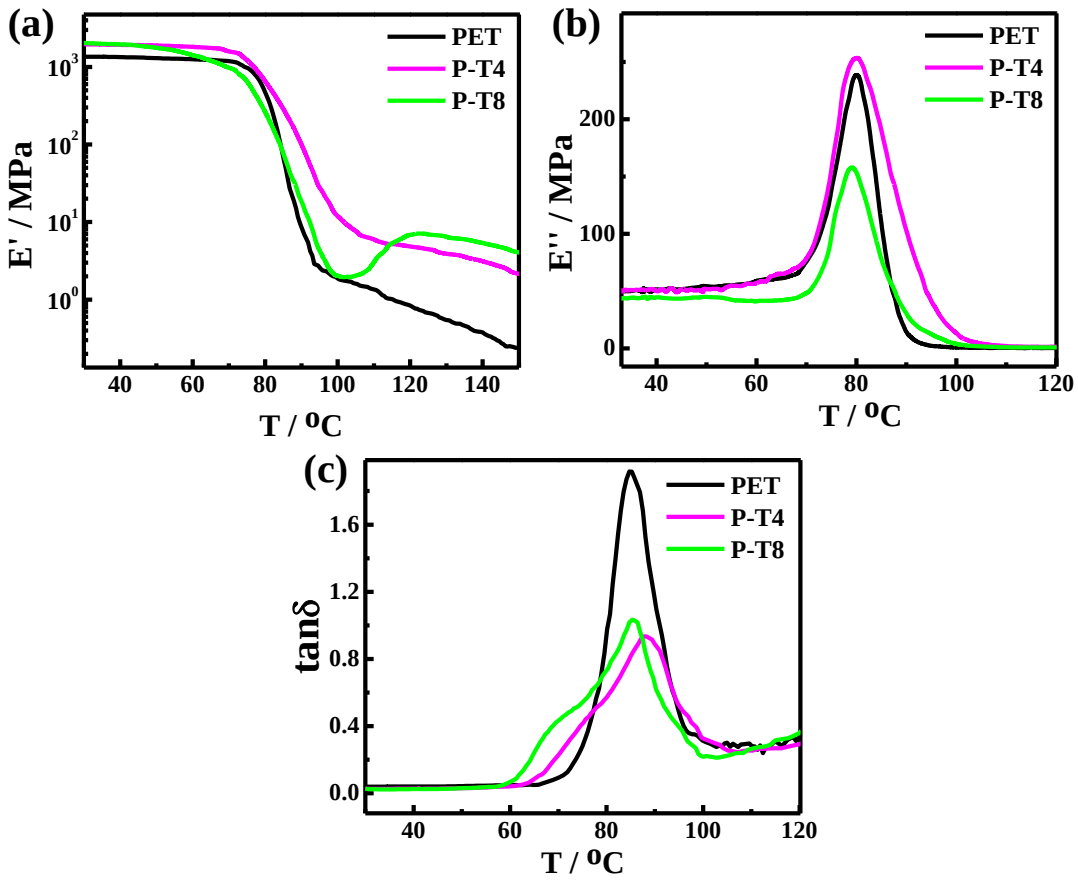

Figure 3.6: *Effect of nanotalc inclusion as measured through dynamic mechanical analyzer on* ***(a)*** *storage modulus;* ***(b)*** *loss modulus and* ***(c)*** *tan δ of PET and its nanohybrids.*

As the temperature increases, the *E'* of nanohybrids starts decreasing. The decrement shifts to comparatively lower temperatures than the pure PET for higher nanotalc loading in the P-T8 nanohybrid. The decrement is also gradual as opposed to steep curve in PET which could be due to the inhomogeneity present in the P-T8 nanohybrids as a result of inhomogeneous dispersion, agglomeration of nanotalc in the PET matrix and/or the impurities present in the nanohybrid at high nanotalc loading. There is an increment in *E'* value of P-T8 after the glass transition which is due to the formation of new ordered crystallites as a result of cold crystallization as reported previously in various studies [196-198]. The loss modulus curve

has been shown in ***Figure 3.6b*** which is indicative of the viscous component. The peak of damping factor tanδ (also called loss factor) is most commonly considered as T_g which is associated with the α relaxations (***Figure 3.6c***). The mobility of the long range segments of amorphous portions in the polymeric materials results in glass transition. The T_g was reported in previous studied from 70 to 140°C of completely amorphous PET or of the amorphous segments of semicrystalline PET [26, 197-201]. The PET shows T_g at 85°C whereas nanohybrids P-T4 and P-T8 show higher T_g at 88°C and 83°C respectively. The higher T_g is because of the restrictions posed by the nanoclay in the segmental mobility of the amorphous portions of polymeric matrix. The peaks of tanδ curves of nanohybrids are significantly broadened and show two steps with lower amplitudes. The broadening of the peaks is due to the dissimilar amorphous structure present in the nanohybrids causing different mobility. The existence of two steps of tanδ peaks for α relaxation represent the possible presence of two types of amorphous structures [198, 202-204]. The lower amplitude of tanδ peaks of nanohybrid indicate that the elastic constituent (*E'*) prevails over the viscous constituents (*E''*). The increment in T_g has also been supported by the DSC results. The values of T_g resulting from DMA and DSC experiments differ due to the processing conditions and methodology.

3.3.8 Effect of stretching on structure

3.3.8.1 2D-Small angle X-ray scattering (SAXS):

The effect of stretching has been observed through 2D-SAXS. The 2D patterns of unstretched and stretched PET and P-T nanohybrid obtained from SAXS have been shown

in ***Figure 3.7a***.The unstretched PET as well as unstretched P–T shows the isotropic ring pattern. This is due to amorphous structure that the polymer matrix bears before stretching.

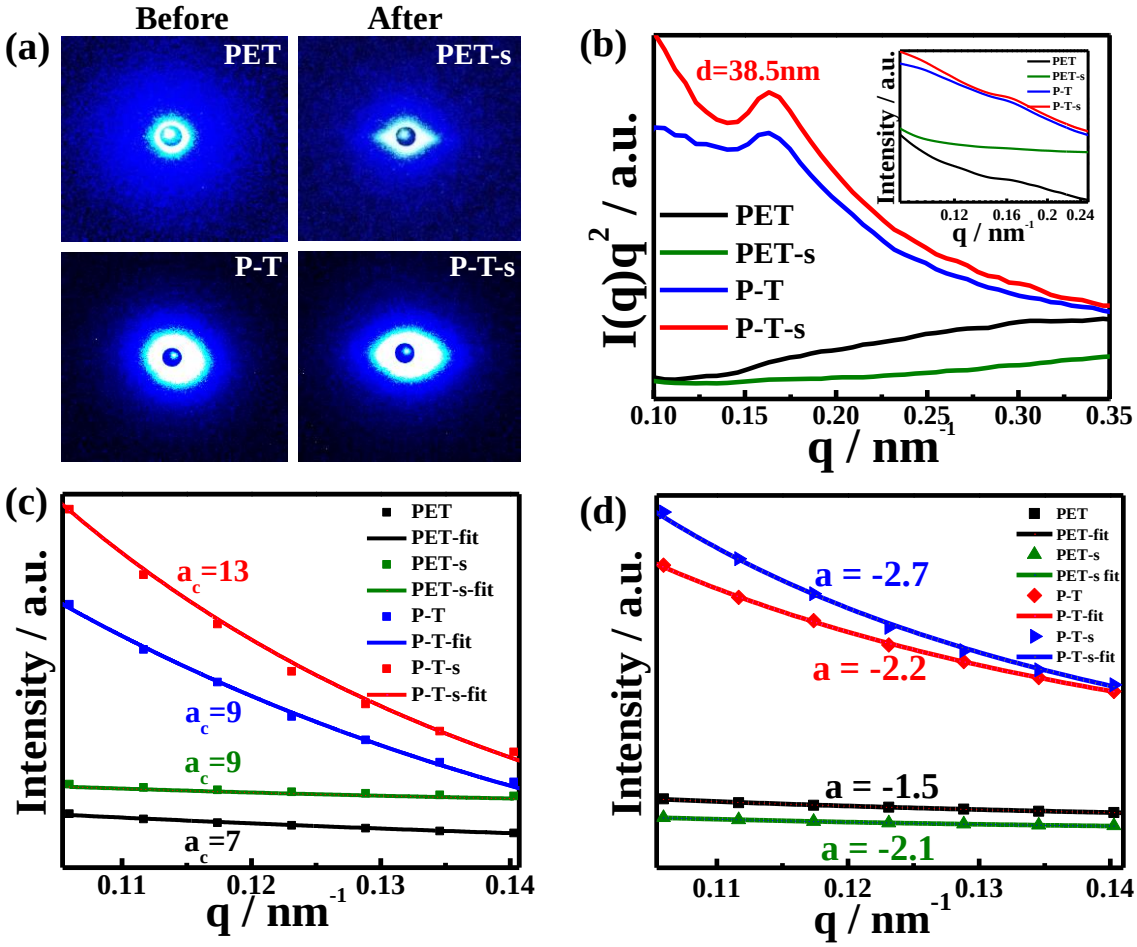

Figure 3.7: *Structural advancement in PET and its nanohybrids containing 4 wt % of filler concentration;* ***(a)*** *2D SAXS images of before and after stretching of the nanohybrid (the stretching is in vertical direction and the stretched samples are denoted with "-s" in addition to pre-existed abbreviation);* ***(b)*** *Lorentz corrected $I(q)q^2$ versus q plots, inset image shows plots of I(q) (scattering intensity) versus (q) (scattering vector);* ***(c)*** *Debye–Bueche fitting of the low value of scattering intensity to get the correlation length values of unstretched and stretched PET and its nanohybrid;* ***(d)*** *Linear fitting of slope values of low q values.*

A streak is formed perpendicular to the loading direction upon stretching the PET as well as P–T nanohybrid. This streak is formed due to the short-range ordering induced by stretching the samples. The streak also results from the fibrils or void elongation which results due to stretching in perpendicular direction [205]. Different mesophases have been reported previously by stretching the polymer [206-208]. Lorentz corrected $I(q)q^2$ versus q plots have been shown in ***Figure 3.7b*** where, $I(q)$ is the scattering intensity and q is the scattering vector. There is a peak at q = 0.16 nm^{-1} in P–T nanohybrids which is due to the short range ordering in the presence of the nanotalc. The characteristic length ($\wedge_c = 2\pi/q_{max}$ where, q_{max} is the wavevector corresponding to the maximum intensity) has been calculated to be 38.5 nm. The intensity of this peak increases on stretching the sample. This shows that the short-range ordering has increased upon stretching the nanohybrid. This is because of the increased ordering due to localized effect through structure formation. The talc particles get partially aligned in the direction of stretching under the force field. The stretching of P–T nanohybrids leads to orientation of talc tactoids in more coherent manner and the enhanced coherency is because of the localized effect. The linear part of the $I(q)$ versus q curve has been fitted with the Debye–Bueche model to calculate the correlation length (***Figure 3.7c***). Debye–Bueche model is given as [173, 209]:

$$I(q) = \frac{A}{(1+a_c^2 q^2)^2} \tag{3.9}$$

Where a_c is the correlation length and A is a constant. The correlation length values are shown in ***Figure 3.7c***. It is evident that the correlation length has increased upon stretching the samples and is comparable to the reported values [210]. The increment in nanohybrid is more than the pure polymer. The elongated structure of the nanotalc under stretching is predominantly responsible for this. The correlation length represents the blob size of the

material. The blob size of the nanohybrid increases because of the elongated structure formation due to the shearing of the talc platelets. The linear slopes of the *log–log* plot of the *I(q)* versus *q* plot has been fitted with the power law equation given as $log_{10}I(q) = A - a log_{10}(q)$, where *a* is the slope of the segment of the lower values of *q*. The values of the slopes for the unstretched and stretched PET are −1.5 and −2.1, whereas P–T nanohybrid has the values of −2.2 and −2.7 for unstretched and stretched samples, respectively (***Figure 3.7d***). The value of the slope for randomly oriented thin disc structure has been reported as −2 [211]. The variation from the reported values can be due to the formation of the tactoids. The increment in slope values upon stretching is attributed to the elongated structure formation because of stretching.

3.3.8.2 Wide-Angle X-ray diffraction (WAXD)

The plots of wide-angle X-ray scattering have been shown in ***Figure 3.8a***. Here, the unstretched PET shows a halo which is due to its amorphous structure. The stretched PET shows peaks at 0.63, 0.52 nm (010), and a small hump at 0.37 nm (100) [206-208]. The peak at 0.63 nm has not been assigned previously and might have risen due to the local structure formation. The unstretched P–T nanohybrid shows a small peak at 0.31 nm which is the peak of pure nanotalc (***Figure 3.8b***). Few peaks appear in the wide-angle X-ray diffraction (WAXD) pattern when the P–T nanohybrids are stretched. The peaks for d-spacing of 0.45 and 0.31 nm of pure nanotalc appear in the stretched P–T nanohybrid with a little shifting. The peak of 0.45 nm shifts to 0.43 nm and peak at 0.31 nm shifts to 0.32 nm. These shifting are due to the short-range ordering in the nanohybrids upon stretching. Intensity of the peaks at 0.37 and 0.52 nm increases and become more intense than pure stretched PET. The

increment in the intensity is due to enhanced coherency in short-range ordering upon stretching the nanohybrid. The nanotalc particles get adhered onto the polymer chains and hence more elongated structure is formed as shown in the schematic of ***Figure 3.8c*** which can explain the appearance of the higher intense peaks. The TEM image of stretched P-T nanohybrid shows partially aligned and elongated talc platelets ***Figure 3.8d.***

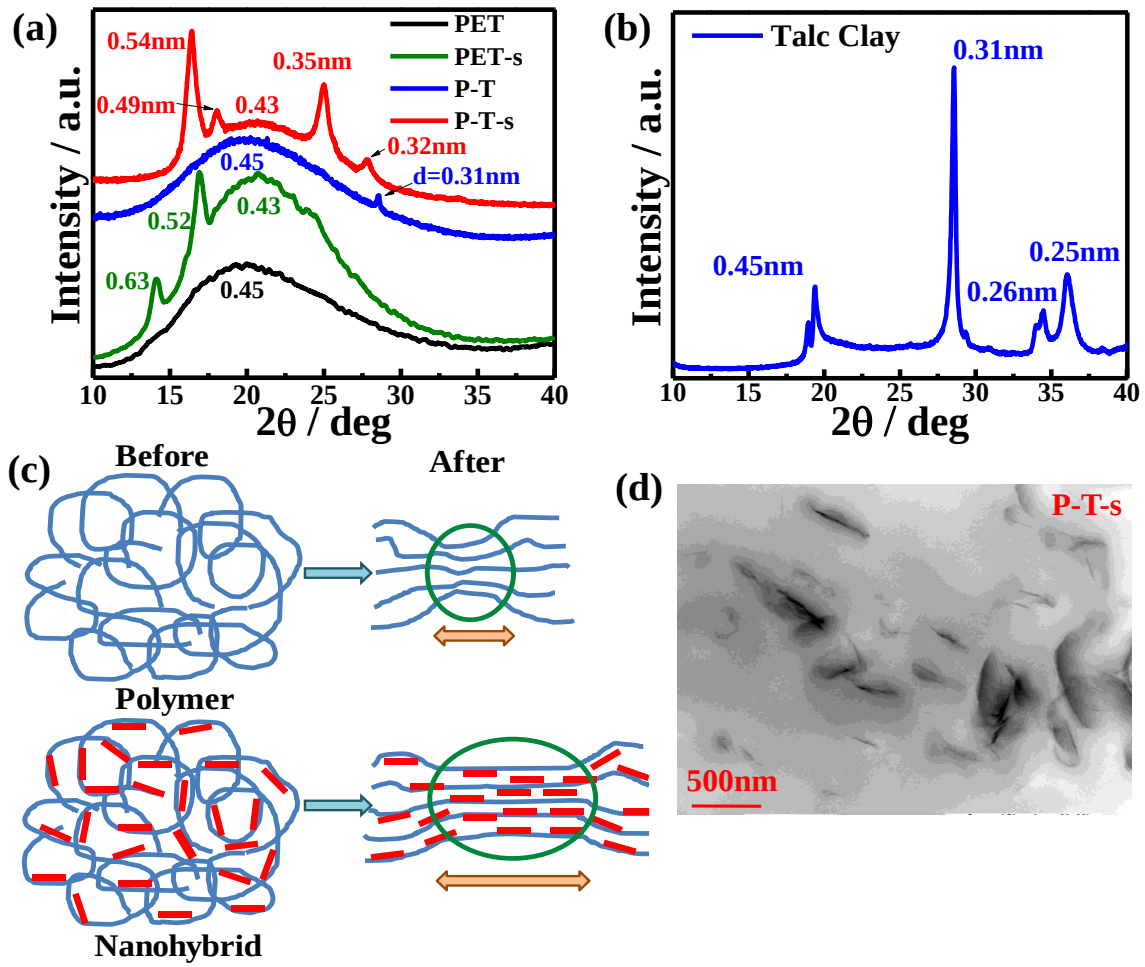

Figure 3.8: ***(a)****WAXD patterns of the unstretched and stretched sample of PET and its nanohybrid;* ***(b)*** *WAXD pattern of pure talc nanoclay* ***(c)*** *schematic representation of the enhancement in short-range ordering due to adherence of nanotalc particles onto the polymer chains after stretching; and* ***(d)*** *TEM images of the stretched P–T (4 wt %) nanohybrid.*

3.3.9 Effect of nanotalc on gas barrier

Transportation of gaseous molecules through PET and its nanohybrids can be visualized through gas permeability. The effect of nanoparticles on the gas barrier properties of PET and its nanohybrids is investigated for different filler concentrations. ***Figure 3.9a*** shows the oxygen transfer rate (OTR) through PET and P–T nanohybrids of different filler concentrations. The permeability values have been shown in ***Table 3.2***. Clearly, the OTR has decreased with increasing filler concentration. P–T nanohybrid films show better gas barrier properties than pristine PET due to better dispersion of 2D nanotalc platelets in polymer matrix. The maximum reduction in permeability value is found to be for 8 wt % filler concentration. OTR has improved up to 64% by incorporating nanotalc in the polymer matrix. Nanotalc sheets block the path of gaseous molecules and make a tortuous path. And thereby make them to travel from a longer path by creating longer tortuous routes as shown in the schematic diagram ***Figure 3.9b***. Better dispersion of nanoparticles and higher level of exfoliation is needed for improvement in barrier properties. The barrier properties achieved are much better than the previously reported data [177]. Microlayering method of preparation needed 32 wt % of macrotalc required for around 72% barrier improvement. Here, for meager, 8 wt % talc has been used to achieve 64% decrement in permeability value. The efficiency of barrier effect does not increase much as compared to lower concentration because of the fact that particles tend to agglomerate at higher filler concentrations. The degree of tortuosity also depends upon the factors such as filler geometry, orientation, degree of exfoliation, and intercalation.

Table 3.2: Permeability values for different concentrations of nanotalc in PET nanohybrids

Sample	Permeability (cc.cm.m^{-2}day^{-1})
PET	0.61 ± 0.03
P-T 1	0.51 ± 0.25
P-T 2	0.42 ± 0.02
P-T 4	0.25 ± 0.01
P-T 8	0.22 ± 0.01

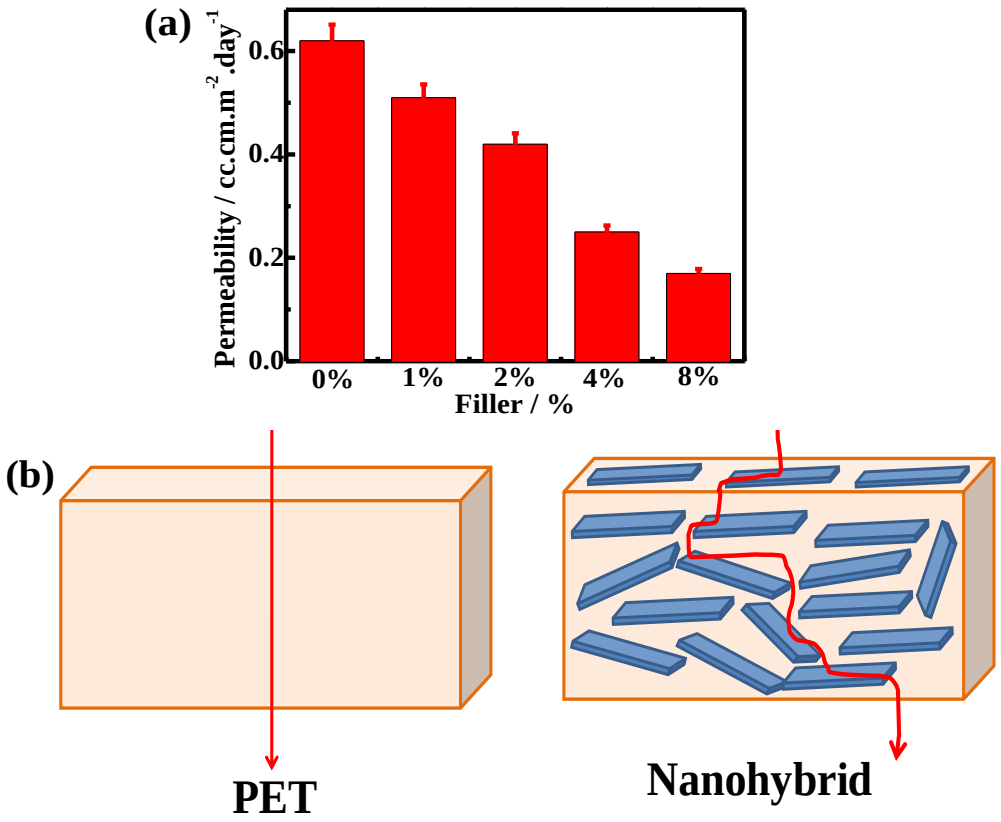

Figure 3.9: (a) *Permeability of PET and its nanohybrids for different filler concentrations;* ***(b)*** *schematic representation of gas molecules path through pure PET and in nanohybrids containing nanotalc which cause the tortuous path for the gas molecules to pass through.*

3.3.10 Theoretical modeling of gas permeability

The gas permeability of a homogeneous pure polymer matrix occurs through diffusion solubility mechanism [212, 213]. The solution diffusion mechanism of a penetrant in a steady state transport is governed by the following relation:

$$P = DS \tag{3.10}$$

where, *P* is the permeability coefficient which depends on the diffusion coefficient (*D*) and solubility coefficient (*S*). The diffusion coefficient describes about the kinetic aspect of the transport while the solubility coefficient relates the penetrant and polymer affinity and describes the thermodynamic aspect of the transport phenomena [213, 214]. For the eq. (11) to be hold true, the value of diffusion coefficient should be independent of the concentration and solubility coefficient should follow the Henry's law. This equation has also been considered often for the gas transport properties of materials reinforced with impermeable nanofillers dispersed in polymer matrix. *P* represents the ongoing volumetric gas flow rate for a fixed area of the membrane in steady state conditions. The nanohybrid films are considered to have better gas barrier properties than a homogeneous system. If the interaction of filler and matrix material is strong and there are no voids present in the material as well as the local characteristics of the matrix material remain unaffected by the presence of filler dispersed in it, then the gas solubility of the composite system can be expressed by the simplest model as described by Picard *et al* [212]:

$$S = (1 - \phi)S_0 \tag{3.11}$$

where, S_0 represents the solubility coefficient of pure polymer, *S* is the solubility coefficient of the composite system and ϕ is the volume fraction of the filler particles. The filler particles

act as an impermeable obstacle and do not allow the gas molecules to pass through them and hence create a tortuous path for the penetrant gas to pass through the nanohybrid film. This reflects in the reduction of diffusion coefficient which is expressed by eq.

$$D = \frac{D_0}{\tau} \tag{3.12}$$

Where, D_0 is the diffusion coefficient of pure polymer, D represents the diffusion coefficient of the nanohybrid film and τ is the tortuosity factor which depends on the particles shape, size and volume fraction of nanofillers and is defined as the ratio of actual distance to the shortest distance travelled by the gas molecule through the nanohybrid film. By combining eq. (11), (12) and (13) one can get the relative permeability *i.e.* the ratio of permeability of the nanohybrid and the permeability of the pure polymer as;

$$\frac{P}{P_0} = \frac{(1-\phi)}{\tau} \tag{3.13}$$

Where, P is the permeability coefficient of the nanohybrid and P_0 is the permeability coefficient of the pure polymer. To describe the tortuosity, different models [212, 215-221] have been proposed in the literature considering different factors contributing in the decrease of permeability value which results from the dispersion of impermeable filler particle in the polymer matrix. Here, Nielsen and Bharadwaj models are used for the fitting of the experimental data.

Nielsen model: This model assumes the platelets to be fully exfoliated and arranged in the polymer matrix as regular array of ribbons of infinite width and thickness [212, 214, 215]. The relative permeability predicted by Nielsen model is given as:

$$\frac{P}{P_0} = \frac{(1-\phi)}{1+\left(\frac{\alpha}{2}\right)\phi} \tag{3.14}$$

Where, $\alpha = l/t$ is the aspect ratio of filler particles, (l = length and t = thickness of the nanoplatelets).

Bharadwaj model: This micromechanical model takes filler particle orientation into consideration. Here, sheet order parameter is included for the orientation direction of fillers and is described as [221]:

$$\frac{P}{P_0} = \frac{1-\phi}{1+\frac{l}{2t}\phi\left(\frac{2}{3}\right)\left(s+\frac{1}{2}\right)} \tag{3.15}$$

where, s is the sheet order parameter and it is defined as:

$$s = \frac{1}{2}\left(3cos^2\theta - 1\right) \tag{3.16}$$

where, θ is the angle between the direction of preferred orientation of nanoplatelets and the sheet normal vector. '*s'* varies from (-1/2) to 1, where 1 stands for perfect alignment, perpendicular to gas flow, (-1/2) for parallel alignment to gas flow and 0 occurs for random orientation of filler particles.

Cussler model: Cussler model assumed the filler platelets were distributed periodically in the polymer matrix in form of several distinct planes. The model assumed oriented array of filler particles placed in regular as well as in random fashion [216, 217]. The model given for random and oriented filler particles was given as:

$$\frac{P}{P_0} = \frac{(1-\phi)}{(1+\frac{\alpha\phi}{3})^2} \tag{3.17}$$

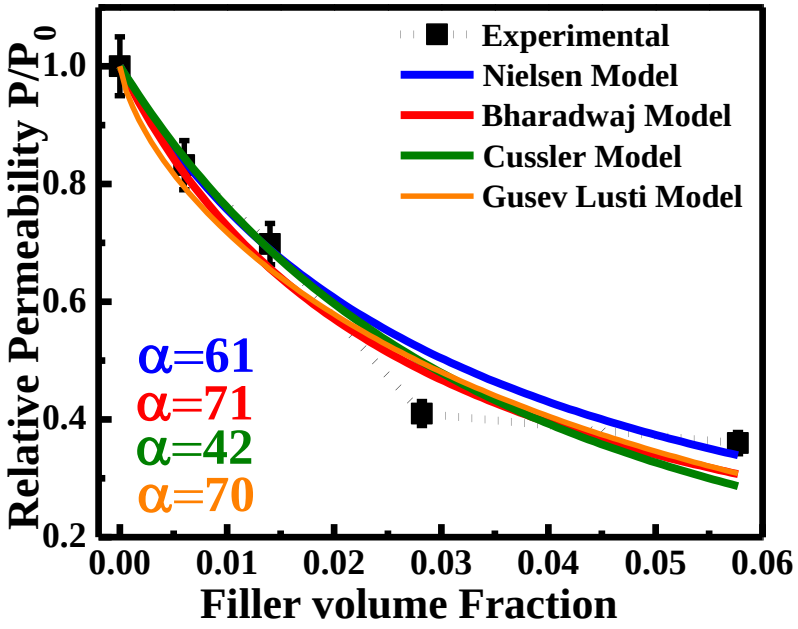

Figure 3.10: *Predictions of permeability values using different fitting models which fit at different aspect ratios (α)*

Gusev Lusti model: This model takes the assumption as the filler dispersed have a circular disk shape with a thickness *'t'* and diameter *'d'*. The filler particles dispersed in matrix are assumed to be random array which are oriented [218]. The model is given as:

$$\frac{P}{P_0} = \frac{(1-\phi)}{\exp[(\frac{\alpha\Phi}{3.47})^{0.71}]} \tag{3.18}$$

The permeability data are fitted to these models using aspect ratio as fitting parameter (***Figure 3.10***). The sheet order parameter for the Bharadwaj model fitting is taken as 1. Nielsen model fits at an aspect ratio of 61 whereas Bharadwaj model fits at 71. Cussler model and Gusev and Lusti models have also been fitted at value of α = 42 and 70. The value of

aspect ratio obtained through fitting is comparable to the literature reported values [179]. The Nielsen model predicts the permeability values very closely for 8% of filler concentration whereas at 4 wt% of nanotalc concentration, the models do not predict the values accurately but under predict than the experimental value. At low concentrations, all the models predict the permeability values closely. The slight deviation in permeability value prediction by micromechanical models (except Nielsen model) at high clay loading occurs due to the presence of agglomeration at high clay percentage, hence the experimental values of permeability do not improve as predicted (for 8 wt % clay loading). For 4wt % the better permeability improvement for experimental result than the predicted values is due to the better dispersion of clay and the strong interaction with the PET matrix. The aspect ratio value varies for different methods due to the reason that every model takes different assumptions and different approaches. The aspect ratio has different effects on different properties. The gas barrier property of a nanohybrid mainly depends on the tortuous path created by the hindrance induced by the presence of nanotalc. Other factors play major role in enhancing the barrier property such as filler geometry, filler particle dispersion, presence of pinholes, cracks, or voids. These factors alter the gas barrier property to a great extent. The interaction of permeate gas to the polymer matrix also affect the test results. If the gas passing through the polymer matrix has any interaction with the same than the effect of the presence of filler particles could not be predicted clearly. Here, we have used oxygen gas as permeate because it is immune to react with the polymer matrix (PET). These models then depend on the aspect ratio (α) and amount of filler concentration (ϕ) only. ϕ is the function of filler concentration and densities of polymer and nanotalc. Hence, α becomes the fitting parameter and one can predict different permeability values by varying different values of α. The fitting value of α cannot be compared to the experimental aspect ratio value obtained

through TEM images. There are many factors which add to determining the actual aspect ratio value such as level of dispersion, exfoliation, and intercalation. Hence, gas barrier property is nicely predicted using various theoretical models for various practical applications.

3.4 Conclusions

The nanohybrids of amorphous thermoplastic PET have been prepared using nanotalc. The notable level of dispersion of nanotalc in the polymer matrix has been examined through TEM analysis. The specific interactions between nanotalc and polymer matrix has been revealed through spectroscopic and thermal measurements. The considerable shifting in FTIR and UV–vis absorption peaks has been observed and dipolar interaction between metal oxide and π-cloud of polymer (benzene ring) is found responsible for greater interactions. Thermal stability of nanohybrids has been found to be improved along with increment of glass-transition temperature of the nanohybrids up to 8 °C. The mechanical properties of the amorphous polymer and nanohybrids have been tested and have shown remarkable improvement. The modulus has shown a progressively increasing trend with increasing talc concentration. The experimental elastic modulus values have been predicted using the theoretical models. Halpin Tsai model has fitted satisfactorily and has predicted the elastic modulus values close to that obtained in experiments. The effect of nanoparticles on the hardness of the nanohybrids has been observed through Vicker hardness test where the VHN has increased considerably in nanohybrids. The MROM and Halpin Tsai model has been used to predict the hardness values of nanohybrids which fit perfectly with the experimental values. The presence of talc on the effect of stretching has been observed extensively through

SAXS and WAXS. The orientational ordering has been observed in the stretched samples and has been found to increase in the presence of nanotalc. Blob size has been calculated by fitting the Debye–Bueche model using the lower wavevector region data. The blob size has increased for stretched samples in the presence of nanotalc in comparison to pure polymer. Gas barrier properties of nanohybrids have significantly been improved as compared to pristine PET. The permeability of nanohybrids have decreased up to 64% using 8 wt % concentration of nanotalc keeping with the increase in tortuous path for the diffusion of penetrant gas molecules. The small amount of nanotalc induce large extent of barrier into the polymer matrix has been due to uniform dispersion of nanotalc in the polymer matrix and the strong interaction between nanotalc and the hydrophobic PET matrix. The gas barrier properties have been extensively studied and different models have been used to predict the experimental values very precisely. Nanotalc inclusion in PET has shown great enhancement in properties without using any additive. A balance among the gas barrier, mechanical, and thermal properties have been achieved using nanotalc whose values have improved significantly for practical applications.